ION ACCELERATION IN NON-STATIONARY SHOCKS

Q. M. Lu*, Z. W. Yang*, B. Lembège† and S. Wang*

*CAS Key Laboratory of Basic Plasma Physics, School of Earth and Space Sciences, University of Science and Technology of China, Hefei, Anhui 230026, China.
†Centre d'étude des Environnements Terrestre et Planétaires, CNRS Université de Versailles-Saint Quentin, Vélizy 78140, France.

Abstract. Previous particle-in-cell simulations have evidenced that quasi-perpendicular shocks are non-stationary and suffer a self-reformation on gyro scale of the incoming ions. In this paper, by separating the incoming ions into reflected and directly transmitted parts, we investigate ion acceleration in a non-stationary perpendicular shock. The results show that shock drift acceleration (SDA) is a dominant acceleration mechanism, while shock surfing acceleration (SSA) mechanism becomes more and more important with the increase of the initial particle energy (both their average final energy and percentage increase). The percentage of reflected ions cyclically varies in time with a period equal to the self reformation cycle.

Keywords: perpendicular shock, shock drift acceleration, shock surfing acceleration, reformation
PACS: 94.05.Pt, 96.50.Fm, 96.50.Pw, 96.50.Vg

INTRODUCTION

Collisionless shocks are of fundamental interests in space and astrophysical plasma, and they are commonly believed to be important sources for high-energy particles. At quasi-parallel shocks, the theory of diffusive shock acceleration (DSA) is quite successful to account for observed energetic particles [1, 2, 3, 4, 5]. The upstream ions reflected by quasi-parallel shocks can go far upstream along the magnetic field line, and excite low-frequency plasma waves which in turn scatter the ions cross the shock back and forth many times. In this way, the ions are accelerated to high energy. However, a similar theory does not work at quasi-perpendicular shocks, where the reflected upstream ions return to the shocks almost immediately due to the gyro-motion in the magnetic field. Therefore, the quasi-perpendicular shocks cannot provide self-produced plasma waves with large spatial/temporal scales similar to ULF waves observed at quasi-parallel waves to scatter the particles.

Shock drift acceleration (SDA) [6, 7, 8] and shock surfing accelerations (SSA) [9, 10, 11, 12] are considered to play important roles in ion accelerations at quasi-perpendicular shocks. In shock drift acceleration, the particles gain energy as their guiding centers move along the convective electric field due to the drift effects of the magnetic field gradient or the curvature of the shock front [13, 14]. In shock surfing acceleration, the particles are reflected by the shock potential, and then they return to the shock front due to the upstream Lorentz force. In this process, these particles are trapped at the shock front and accelerated by the convective electric field. They may repeat the process several times until they have acquired sufficient kinetic energy to overcome the macro-

CP1183, *Shock Waves in Space and Astrophysical Environments*
edited by X. Ao, R. H .Burrows, and G. P. Zank

scopic potential barrier at the shock front [15, 16, 17, 18]. With hybrid simulations, Burgess et al. [19] have analyzed the ion accelerations at quasi-perpendicular shocks by separating the incoming ions into transmitted and reflected parts. They found that none of the reflected ions comes from the core of the upstream velocity distribution, and those reflected ions form the high energy tail of the downstream distribution. Lipatov and Zank [20] investigated shock surfing acceleration of pickup ions at perpendicular shocks, and found that the width of shock ramp is the key factor determining the efficiency of shock surfing acceleration. Lever et al. [21] compared the efficiency of shock surfing and shock drift acceleration mechanisms for different widths of shock ramp, and they demonstrated that SSA process predominates when the width of shock ramp is below a critical value. However, the used ramp width was not obtained self-consistently, which has strong consequences as shown in the present study.

In the above studies, the structures of quasi-perpendicular shocks are based on hybrid simulations, the used space resolution (and the minimum width of the shock ramp) is roughly $\sim 0.5-1c/\omega_{pi}$ (where c/ω_{pi} is the ion inertial length). Recently, particle-in-cell simulations clearly evidence that quasi-perpendicular supercritical shocks are non-stationary and suffer a self-reformation on the gyro scale of the incoming proton due to the accumulation of reflected ions (foot formation) [22, 23, 24, 25, 26, 27, 28]. In this paper, by separating ions into transmitted and reflected parts, we investigate the ion acceleration mechanisms with different initial energy in the non-stationary perpendicular shock obtained from one-dimensional (1-D) PIC simulations.

The paper is organized as follows. In Section 2, we briefly describe the simulation model. The simulations results are presented in Section 3. The discussion and conclusions are summarized in Section 4.

SIMULATION MODEL

In this paper, a self-consistent perpendicular shock profiles are obtained from 1-D PIC simulations. The initial and boundary conditions are similar to those already explained in details in [24], and the shock is initiated by a magnetic piston (applied current pulse). Therefore, the shock geometry is defined in the upstream frame: the shock propagates along the x direction and an upstream magnetic field B_0 is applied along the z direction. All dimensionless quantities are indicated by a tilde "$\sim$" and are normalized as follows. The spatial coordinate is $\tilde{x} = x/\Delta$; velocity $\tilde{v} = v/\omega_{pe}\Delta$; time $\tilde{t} = \omega_{pe}t$, electric field $\tilde{E} = eE/m_e\omega_{pe}^2\Delta$; magnetic field $\tilde{B} = eB/m_e\omega_{pe}^2\Delta$. The parameters Δ, ω_{pe}, m_e and e are, respectively, the numerical grid size, the electron plasma frequency, the electron mass and the electric charge. All basic parameters are identical to those used in [29]: plasma box size length $L_x = 4096$; velocity of light $\tilde{c} = 3$, and mass ratio $m_i/m_e = 84$. Initially, the particle density is $n_e = n_i = 50$ at each grid point. With the decrease of electron/ion temperature ratio, the non-stationarity of the shock will be less obvious [29], and the electron/ion temperature ratio $T_e/T_i = 1.58$ is chosen in order to investigate the particle acceleration at a reforming shocks. The ambient magnetic field is $|\tilde{B}_0| = 1.5$. The shock front is propagating along x direction in a supercritical regime with the average Mach number about ($M_A = 5.24$), where $M_A = \tilde{V}_{shock}/\tilde{V}_A$ is determined in the upstream plasma (i.e. simulation) frame; the Alfven velocity $\tilde{V}_A$ is equal to 0.16. For these initial condition,

TABLE 1. Table 1. Upstream Plasma Parameters Defined for PIC Simulations

		Electrons	Ions
Thermal velocity	$\tilde{V}_{thx,y,z}$	0.2	0.017
Debye length	$\tilde{\lambda}_D$	0.2	0.16
Larmor gyro radius	$\tilde{\rho}_c$	0.4	2.91
Inertia length	$\tilde{c}/\tilde{\omega}_p$	3.0	27.5
Gyro frequency	$\tilde{\omega}_c$	0.5	0.006
Plasma frequency	$\tilde{\omega}_p$	1.0	0.11
Gyro period	$\tilde{\tau}_c$	12.55	1055.46
Plasma beta	$\tilde{\beta}$	0.0355	0.0225

the plasma parameters are summarized in Table 1 for both electrons and ions.

SIMULATION RESULTS

The time evolution of the perpendicular shock is shown in Figure 1, which plots the magnetic field $\tilde{B}_z$ within the spatial range $\tilde{X} = 4600$ to 5900. The shock is non-stationary, and a self-reforming shock front is observed. The black curve in the figure describes the ramp position of the shock ramp. The shock is in supercritical regime characterized by a noticeable density of reflected ions responsible for the formation of the foot located upstream of the ramp and for the overshoot. At $\tilde{t} = 650$, the shock front is at about $\tilde{X} = 4600$. Later at about $\tilde{t} = 800$, the reflected ions have accumulated in the foot with a percentage relatively high so that the foot amplitude increases and reaches a value comparable to that of the “old" ramp. Then, a “new" shock ramp builds up and starts reflecting new incoming ions. The “new" shock front is well formed around $\tilde{X} = 4850$ at about $\tilde{t} = 950$. Simultaneously, the “old" shock front becomes weaker and weaker and is located downstream of the "new" front. The shock front is characterized by a self-reformation with a cyclic period about $288\omega_{pe}^{-1} \approx 1.73\Omega_{ci}^{-1}$.

In this paper, we investigate in details ion acceleration in this pre-defined non-stationary perpendicular shock with test particle simulations. We follow the trajectories of 12000 particles, which are released with different kinetic energy. For all test particle simulations performed herein, the incoming ions are distributed evenly in the region $100 < \tilde{x}_i - \tilde{x}_{ramp} < 1420$ at a chosen starting time $\tilde{t} = 628$, where $\tilde{x}_i$ is the position of the ion i, and $\tilde{x}_{ramp}$ is the position of the shock ramp, which is determined by $|\partial \tilde{B}_z^2/\partial x|_{max}$ (inflexion point in the ramp of B_z profile). In the simulation, the width of the upstream region filled with test particles is sufficiently large, and it takes about 5 shock reforming cycles to advect these particles through the shock. If no explicitly mentioned, the distribution of the test particle velocities is initially described as shell function, and ions only differ by their phase angles on the shell. All particles have same kinetic energy, and the shell radius defines the kinetic energy of the particles. Here, the propagating shock is injected with a velocity equal to that measured in the PIC simulation, its instantaneous Mach number can differ from the average value ($M_A = 5.24$).

We separate the upstream ions into two groups: the reflected (R) ions and directly

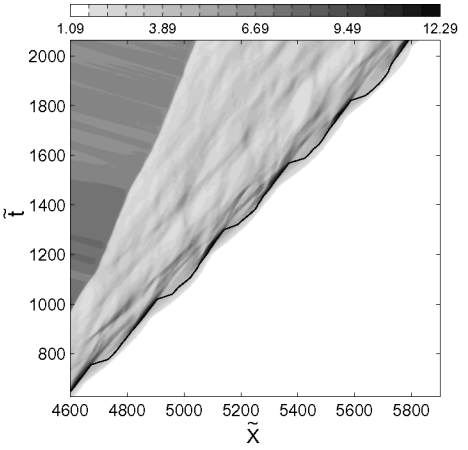

FIGURE 1. The time evolution of $\tilde{B}_z$ versus $\tilde{X}$. The black curve describes the position of the shock ramp (the ramp position is the position of the main ramp, which has larger $\tilde{E}_x$ than the other).

transmitted (DT) ions, and describe their dynamics separately. The reflected ions have the following characteristics: after being reflected (i) their velocity in the x direction $\tilde{v}_{ix}$ is larger than the shock propagating speed $\tilde{V}_{shock}$, and (ii) they are located upstream the ramp $\tilde{x}_i > \tilde{x}_{ramp}$. Here, the shock propagating speed is defined as the moving speed of the shock ramp. Further more, the R ions can be divided into two subpopulations by using a simple criterion in order to exact some relevant information from a statistical analysis [21]: the SDA ions are accelerated by the shock drift mechanism, and they are primarily reflected by the Lorenz force, i.e., in the ramp $\tilde{E}_x < \tilde{v}_{iy}\tilde{B}_z/\tilde{c}$. SDA ions do return upstream once before passing through the shock front. The SSA ions are accelerated by the shock surfing acceleration, and they are primarily reflected by electrostatic force, i.e., in the ramp $\tilde{E}_x \geq \tilde{v}_{iy}\tilde{B}_z/\tilde{c}$. In contrast with SDA process, SSA ions show multiple surfing reflections with a small normal amplitude as described by [21].

The ion dynamics can be identified clearly by tracing their trajectories, and Figure 2 shows four typical ion trajectories. In the figure, the left column describes the ion trajectories, and the right column shows the their kinetic energy. In Figure 2(a), the ion firstly undergos SSA from A1 to B1 since $\tilde{E}_x > \tilde{v}_{iy}\tilde{B}_z/\tilde{c}$ at the reflected point A1. Then the ion interacts with the new ramp of the shock at B1 where it is accelerated to higher energy and then transmits to downstream. In Figure 2(b), the ion first suffers SDA process from from A2 to B2 due to $\tilde{E}_x < \tilde{v}_{iy}\tilde{B}_z/\tilde{c}$ at the reflected point B2. Then the ion interacts later with the new ramp of the shock at C2 and succeeds to be transmitted. Figure 2(c) describe an ion multi-stage acceleration. In figure 2(c), from A3 to B3 the ion first suffers an SDA acceleration since $\tilde{E}_x < \tilde{v}_{iy}\tilde{B}_z/\tilde{c}$ at the reflected point B3. From B3 to C3, and then returns upstream. It hits the ramp at a time between A3 and B3 when the overshoot is the highest (indicated by the vertical white line) and then describes a large Larmor orbit upstream. At last, it interacts again with the shock front around C3 and goes downstream. Figure 2(d) shows an ion which directly transmits into the downstream,

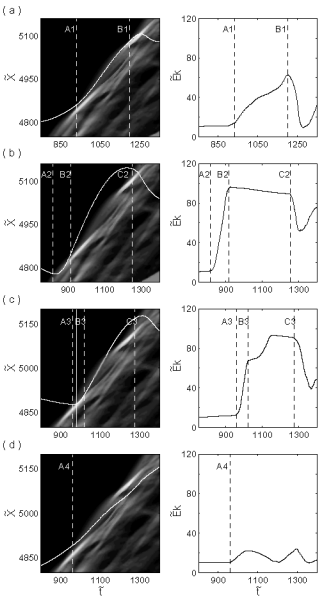

FIGURE 2. Four typical ion trajectories (left column) and kinetic energy (right column) versus time for the time-reforming shock regime. The vertical dash lines denote some key points.

and no obvious acceleration is found. In general, the ions can be accelerated to high energy with SSA, SDA or multi-stage acceleration. These various results confirm again (i) the strong impact of the shock front non-stationarity on the resulting ion dynamics; (ii) that initial SDA process seems to provides the highest resulting energy gain; (iii) the necessity to include the overall width of the varying shock front for analyzing the resulting ion dynamics (and not only the ramp).

Figure 3 shows the domain in (gyro-phase ϕ and pitch-angle θ) in the velocity space for the incident ions undergoing SDA, SSA or DT processes. Since some ions undergo multi-stage acceleration, we identify the type of ion acceleration when ions interact with the main shock ramp for the first time. With the increase of the radius, more particles are accelerated with SSA mechanism, while the SDA mechanism plays an important role for ions with both lower and higher initial energy. The DT, SSA and SDA ions tends to concentrate in the region where ϕ are around 270^o, 45^o and 135^o, respectively. SDA, SSA or DT ions are clearly separated due to the nonstationarity of the shock front. In general, the source of SSA ions at a reforming shock is still consistent with the theoretical results of previous papers [18, 21].

Figure 4 shows (a) the downstream average kinetic energy and (b) the percentage of the SDA, SSA and DT particles as a function of the shell radius. The average kinetic energy and the percentage of the SDA, SSA and DT particles are calculated when their positions are between $\tilde{x}_{ramp} - 500 < \tilde{x}_i < \tilde{x}_{ramp} - 100$ at $\tilde{t} = 2064$. For the SDA ions, the average kinetic energy approximately increases linearly with the initial energy, their

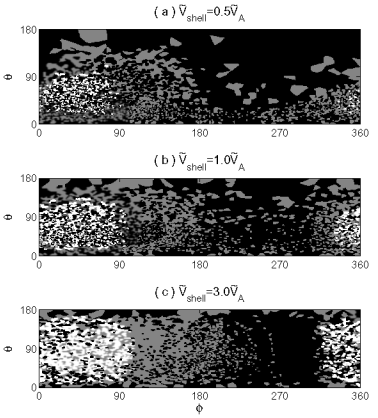

FIGURE 3. Angular domain in ϕ—θ velocity space for SDA (white), SSA (gray) and DT (black) ions for (a) $\tilde{V}_{shell} = 0.5\tilde{V}_A$, (b) $\tilde{V}_{shell} = 1.0\tilde{V}_A$ and (c) $\tilde{V}_{shell} = 3.0\tilde{V}_A$.

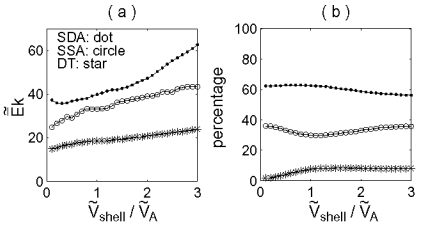

FIGURE 4. (a) The average kinetic energy of SDA (dots-line), SSA (circles-line) and DT (stars-line) ions in downstream and (b) their percentage as a function of their initial radius of the shell distribution. Results are obtained for the time-reforming shock regime.

percentage also increase. This is in agreement with the increase of the angular range spreading as $\tilde{V}_{shell}$ increase. For the SSA ions, because the SSA ions may suffer multi-stage acceleration at the complicated self-reformation shock front, the average kinetic energy increase smoothly with the increase of the initial energy. At the same time, the number of SSA ions also increases with the increase of the initial energy and therefore becomes more and more important. The results are consistent with Figure 3, the larger the radius is, the more particles are accelerated with the shock surfing mechanism.

Figure 5 describes the time evolution of the maximum values of (a) $\tilde{E}_x$ and (b) $\tilde{B}_z$ between $\tilde{x}_{ramp} - 20$ and $\tilde{x}_{ramp} + 20$, and the percentage of the reflected ions in the region $\tilde{x}_{ramp} < \tilde{x}_i < 2L_x$ for (c) the shell distributions and (d) Maxwellian distributions. Obviously, the cyclic period of the reflected ions percentage is equal to that of the shock front self-reformation. With the increase of the initial energy, the effects of the shock non-stationarity gradually decreases. These results show that variation of the percentage of the reflected ions is stronger for small shell radius or thermal velocity (Maxwellian distribution).

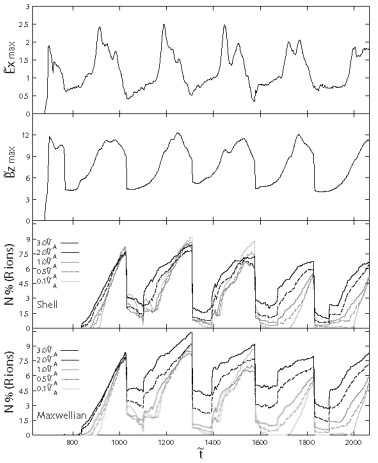

FIGURE 5. Time history of the maximum values of the electrostatic filed $\tilde{E}_{x\ max}$ and the magnetic field $\tilde{B}_{z\ max}$ around the shock ramp, and of the number of the reflected ions. Results are obtained for different radii (shell distribution) and thermal velocity (Maxwellian distribution), respectively.

CONCLUSIONS AND DISCUSSION

Previous particle-in-cell simulations have already evidenced that quasi-perpendicular shocks are non-stationary and can self-reform on gyro scale of the incoming ions. In this paper, we separate the incoming ions into the reflected and directly transmitted parts during their interaction with the shock front, and then investigate the mechanisms of ion acceleration in non-stationary perpendicular shock. Most energetic particles correspond to the reflected ions which are accelerated by SSA and SDA mechanisms. The ion dynamics depends largely on the structures of the shock at the time incoming ions interact with the shock front. Therefore, as the shock evolves with time, the number of the reflected ions and the resulting energy gain strongly vary, the dynamics of particles is more complicated than in stationary shocks.

The above conclusions are obtained by using test particles with shell velocity distributions of different radii. This simple approach is helpful before considering more realistic Maxwellian distributions, because Maxwellian distribution is a weighted superposition of a series of shell velocity distributions with different radii. In extension to the previous results of hybrid simulations [19], we also find (i) whether a given ion is accelerated primarily depends on the time at which ions interact with the shock front, and (ii) energetic particles (SSA and SDA reflected ions) come from a limited portion of the incident distribution, rather than being randomly selected. The accelerated mechanisms of the reflected ions by the non-stationary shocks discussed in this paper may provide a candidate of the pre-acceleration mechanisms that can initiate the diffusive shock acceleration in the quasi-perpendicular shocks, and accelerate ions to even higher energy.

ACKNOWLEDGMENTS

This research was supported by the National Science Foundation of China (NSFC) under grants 40874075, 40725013, 40674093 and Chinese Academy of Sciences KJCX2-YW-N28. The initial 1D PIC simulations have been performed on the supercomputer of IDRIS center located at Orsay(near Paris).

REFERENCES

1. M. A. Lee, *J. Geophys. Res.* **88**, 6109–6119 (1983).
2. R. D. Blandford, and D. Eichler, *Phys. Rep.* **154**, L1–L75 (1987).
3. G. Li, G. Zank, and W. K. M. Rice, *J. Geophys. Res.* **108**, A21082 (2003).
4. J. Giacaclone, *Astrophys. J.* **609**, 452–458 (2004).
5. G. P. Zank, G. Li, V. Florinski, Q. Hu, D. Lario, and C. W. Smith, *J. Geophys. Res.* **101**, A06108 (2006).
6. P. D. Hudson, *Mon. Not. R. Astron. Soc.* **131**, 23 (1965).
7. G. M. Webb, W. I. Axford, and T. Terasawa, *Astrophys. J.* **270**, 537–553 (1983).
8. R. B. Decker, *Space Sci. Rev.* **48**, 195–262 (1988).
9. R. Z. Sagdeev, *Rev. Plasma Phys.* **4**, 23–91 (1966).
10. A. S. Lipatov, G. P. Zank, and H. L. Pauls, *J. Geophys. Res.* **103**, 29679–29696 (1998).
11. D. Ucer, and V. D. Shapiro, *Phys. Rev. Lett.* **87**, 075001 (2001).
12. D. Ucer, and V. D. Shapiro, *Phys. Lett.* pp. 163–167 (2005).
13. R. B. Decker, and L. Vlahos, *J. Geophys. Res.* **90**, 47–56 (1985).
14. S. V. Chalov, *J. Geophys. Res.* **106**, 18667–18675 (2001).
15. G. P. Zank, H. L. Pauls, I. H. Cairns, and G. M. Webb, *J. Geophys. Res.* **101**, 457–477 (1996).
16. M. A. Lee, V. D. Shapiro, and R. Z. Sagdeev, *J. Geophys. Res.* **101**, 4777–4789 (1996).
17. M. A. Lee, *Astrophys. Space. Sci.* **264**, 497–508 (1999).
18. V. D. Shapiro, and D. Ucer, *Planet Space Sci.* **51**, 665–680 (2003).
19. D. Burgess, W. P. Wilkinson, and S. J. Schwartz, *J. Geophys. Res.* **94**, 2503–2504 (1989).
20. A. S. Lipatov, and G. P. Zank, *Phys. Rev. Lett.* **82**, 3609–3612 (1999).
21. E. L. Lever, K. B. Quest, and V. D. Shapiro, *Geophys. Res. Lett.* **28**, 1367–1370 (2001).
22. D. Biskamp, and H. Welter, *Phys. Rev. Lett.* **28**, 410–413 (1972).
23. B. Lembege, and J. M. Dawson, *Phys. Fluids.* **30**, 1767–1788 (1987).
24. B. Lembege, and P. Savoini, *Phys. Fluids.* pp. 3533–3548 (1992).
25. N. Shimada, and M. Hoshino, *Astrophys. J.* **543**, L67–L71 (2000).
26. H. Schmitz, S. C. Chapman, and R. O. Dendy, *Astrophys. J.* **579**, 327–336 (2002).
27. M. Scholer, I. Shinohara, and S. Matsukiyo, *J. Geophys. Res.* **108**, A11014 (2003).
28. K. Nishimura., H. Matsumoto, H. Kojima, and S. P. Gary, *J. Geophys. Res.* **108**, A51182 (2003).
29. T. Hada, M. Oonishi, B. Lembege, and P. Savoini, *J. Geophys. Res.* **106**, A61223 (2003).